AIAA JOURNAL
Vol. 42, No. 7, July 2004

Laminar Lifted Flame Speed Measurements for Aerosols of Metals and Mechanical Alloys

Y. Shoshin* and E. L. Dreizin†
New Jersey Institute of Technology, Newark, New Jersey 07102

This research develops and validates a novel experimental methodology for measurements of laminar flame speed of metal-air aerosols. The methodology is based on a recently developed laminar, lifted flame aerosol burner (LLFAB) using electrostatic fluidization to produce metal aerosol between the electrodes of a plate capacitor. An aerosol jet directed vertically up, and decelerating in a stagnant gas environment is produced. The jet is ignited, and the position of the propagating downward flame is stabilized at a location where the flame speed becomes equal to the jet velocity with the opposite sign. Therefore, the flame speed determines the vertical location of the lifted flame. Aerosol flame speed measurements using LLFAB are compared vs earlier measurements using Bunsen burner and flame tube in microgravity. The developed technique was used to compare the flame speed for pure aluminum and magnesium powders vs flame speed for a set of aluminum-based mechanical alloys using Mg, Ti, Zr, Li, MgH_2, or C as alloying elements. It was observed that the flame speeds for all of the tested alloys, except the one with carbon, are higher than that of the pure aluminum aerosol.

Introduction

METALS are routinely added to propellants and other energetic formulations to increase the combustion enthalpy, flame temperature, and specific impulse. Current active research is is aimed to develop new metal-based fuel additives with higher burn rates as compared to commercial metal powders.[1,2] Many types of novel materials under development, for example, different alloys, coated metal powders, and various surface morphology powders are currently available in small quantities. Extensive testing of their performance is needed before efforts on the scaled up commercial production of these materials can be justified. Therefore, reproducible, simple, and theoretically tractable laboratory techniques are needed for measuring one or more of the combustion parameters of such powders.

For gaseous flames, burning velocity defined as the velocity at which unburned gases move through the combustion wave in the direction normal to the flame surface[3] serves as a fundamental combustion parameter. Burning velocity is expressed through the chemical reaction rate and is relatively simple to measure using Bunsen burner, flame tube, or other premixed flame experimental techniques.[4] One of the critical requirements for an accurate experiment on measuring burning velocity is that the dimension of the produced flame must be much greater than the flame thickness. This requirement is readily satisfied for most premixed gaseous flames with submillimeter thickness. However, it is hardly achievable in a laboratory for most aerosol flames for which the flame thickness could vary from few millimeters to several centimeters, depending on material and particle size. It is also very difficult to produce laminar aerosol flows of the required large cross section without significant agglomeration and settling of the aerosol particles entering the flame.

Literature analysis showed that two experimental approaches were used systematically to measure speeds of laminar aerosol flames and respective burning velocities. Pioneering work by Cassel et al.[5] and Cassel[6] advanced recently by Goroshin et al.,[7–9] explored applicability of Bunsen burner for characterization of aerosol flames. Some interesting trends were established, which distinguished premixed aerosol flames from the gaseous flames, for example, the independence of flame speed on the equivalence ratio in the fuel-rich burning regime.[6,8] At the same time, experimental difficulties of producing large-diameter laminar aerosol flows limited the experiments to very few types of fine metal powders with narrow size distributions. Production of a stable Bunsen cone was found to be impossible for powders with wider size distributions, coarser powders, and many heterogeneously reacting materials. In addition, early Cassel reports[6] showed that the burning velocity measurements obtained using this technique depend on the nozzle diameter. Recently, Goroshin reported that, even for the same nozzle, different burning velocities are being measured at different gas flow rates.[9] It is unclear why the measured burning velocity depends on the Bunsen burner geometry and gas flow rate. However, it is clear that the burning velocities for metal aerosols determined using Bunsen burner cannot be used as fundamental characteristics of premixed aerosol flames.

Another technique used for measurements of aerosol burning velocities is the flame propagation in a tube in normal gravity[10] and microgravity[11] environments. Using flame propagating in a tube in microgravity removes many problems typical for a multiphase flow combustion experiment, but it is unacceptable for mainstream laboratory measurements necessary to characterize a variety of materials. In addition, although it is relatively simple to establish a proper scale, laminar aerosol flame in microgravity, the diagnostics of such a flame is very difficult both because of its large size and because of general limitations of a microgravity experiment.

Note that the fundamental significance of burning velocity for aerosol flames might not be as clear as it is for gaseous flames. For many aerosols, flame propagation rate may be determined by the processes governing particle ignition that have different rates and mechanisms and that occur at lower temperatures than particle combustion, often described as a quasi-steady process. These ignition processes are often driven by relatively slow, heterogeneous reactions with rates limited by the condensed-phase transport processes and with only moderate increase in the particle temperature. Following this reaction stage, a rapid increase in the temperature and transition to full-fledged combustion occurs when vapor-phase transport or chemical kinetics processes control the burning rates. For example, aluminum particles were reported[12–16] to ignite in a temperature range of 900-2300 K, depending on particle size and heating rate, but aluminum particle combustion occurs at about 3000 K (Refs. 17 and 18). It was shown for boron[19] and more recently, for aluminum,[20] that a reasonable global particle combustion model can be produced

Received 22 August 2003; revision received 10 December 2003; accepted for publication 2 February 2004.

*Postdoctoral Researcher, Department of Mechanical Engineering, University Heights.

†Associate Professor of Mechanical Engineering, Department of Mechanical Engineering, University Heights. Member AIAA.

by describing separately low-temperature, heterogeneous processes leading to ignition and rapid, vapor-phase combustion processes. Once ignited, moving aerosol particles continue burning, so that an extended flame zone is formed. The particle burn rate within the extended flame zone may not be directly associated with the processes of particle ignition affecting the flame propagation rate. Thus, the connection between the fuel burn rate and premixed flame burning velocity is not as well defined as it is for gaseous flames.

A directly measurable parameter describing combustion of metal-based fuels in laboratory experiments (and normally used to derive burning velocity) is the speed of flame propagation through the powder aerosolized in a gaseous oxidizer. Although the flame speed is usually apparatus dependent, it could still be used to characterize and compare combustion behaviors of different aerosols if the same apparatus were used to produce different aerosol flames. As already noted, both Bunsen burner and microgravity flame tube techniques are poorly suited for evaluation of a wide range of polydisperse aerosols of novel materials. This work is aimed at the development and validation of a novel experimental technique for measurements of laminar flame speeds of metal–air aerosols. The effects of aerosol jet size, gas flow rate, oxygen concentration, and aerosol mass concentration are considered. The technique is validated by flame speed measurements for Al and Mg aerosols. The technique is used to assess combustion behavior of a set of recently synthesized Al-based mechanical alloys.

Experimental

Production of Aerosol Flame

The experimental technique is based on a recently developed laminar, lifted flame aerosol burner (LLFAB)[21] using electrostatic fluidization to produce a metal aerosol between the electrodes of a plate capacitor.[22] For complete presentation, a schematic diagram of the LLFAB reported elsewhere[21,23] and the experimental apparatus used in this work are shown in Fig. 1. A batch of electrically conductive powder is placed on the lower capacitor plate that has a concave shape and serves as a powder reservoir. A high dc voltage is applied to the electrodes, and an aerosol is formed as a result of recharging of metal particles on particle–electrode collisions and Coulomb forces exerted on charged particles in the capacitor's electric field. It was found that with adequate initial powder loading and sufficiently high voltage, the aerosol number density within the capacitor is controlled only by the applied voltage and can readily be maintained constant for 10–100 s (Ref. 21) (depending on the mass of the powder loaded and aerosol flow rate through the nozzle), that is, long enough to make a flame speed measurement. The capacitor is placed inside a sealed chamber, and its top electrode also serves as the top flange of the chamber. A gas flow is introduced between the plates as shown in Fig. 1. The gas is fed from a pressurized vessel in which a desired oxidizer gas composition is prepared. Air and various oxygen–nitrogen mixtures were used in this project. The gas exits the chamber through a small hole in the top electrode producing a laminar jet. Thus, a vertical aerosol jet is produced in which the particle number density and the particle/gas velocity are controlled independently by a dc voltage and gas flow rate, respectively. The gas flow rate was measured using a rotameter calibrated for each gas mixture using a soap bubble method. The independent controls of the particle number density and jet velocity is a unique advantage of this apparatus as compared to similar devices using fluidized bed to produce an aerosol, for example, in Refs. 5–10. A 0.8-mm-diam opening in the top electrode was used in this project for most of the measurements, whereas a 1.6-mm opening was also used in some tests described later. A very slow shroud flow of the same gas as fed through the burner is also produced, as shown in Fig. 1, to provide consistent flame environment and to stabilize the aerosol jet.

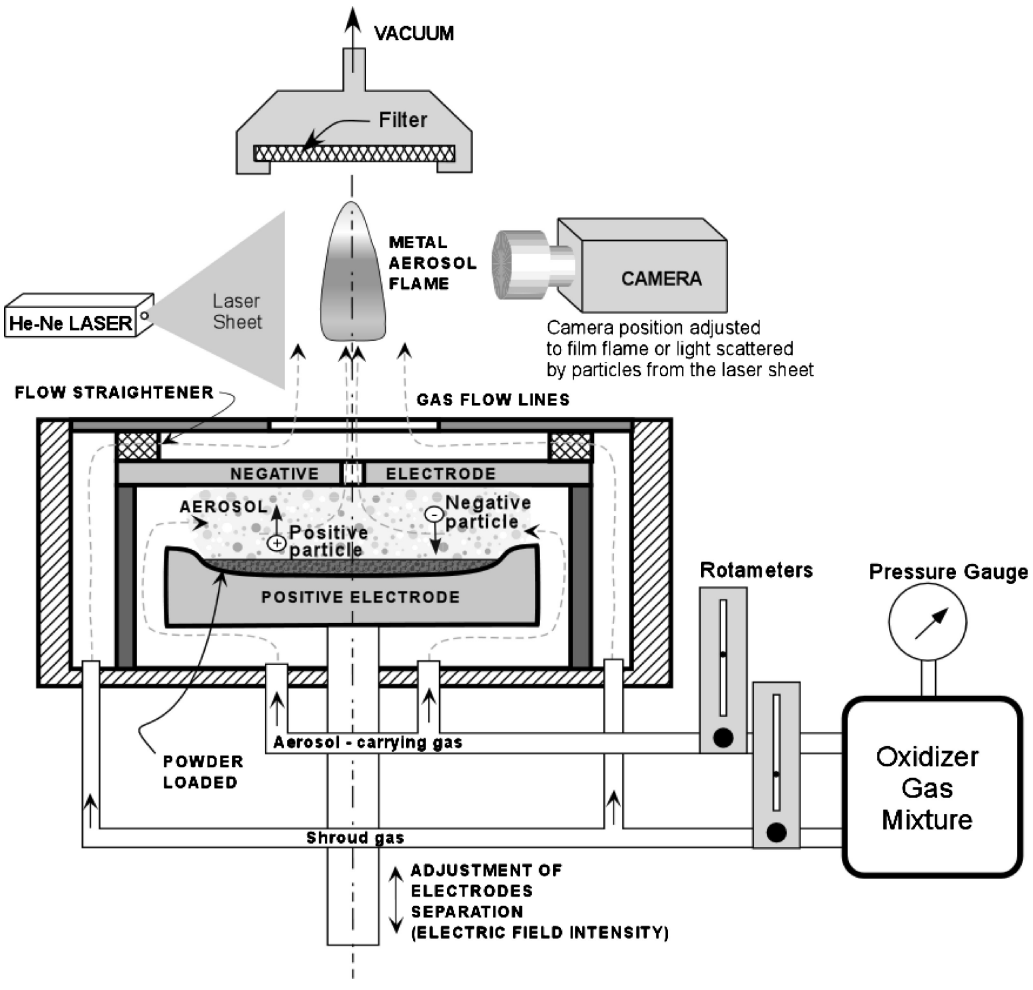

Fig. 1 Schematic diagram of LLFAB and experimental setup.

Because the velocity of the shroud flow is only few centimeters per second, the aerosol jet is produced in an essentially stagnant gas environment, and therefore, it is decelerated due to the drag forces. When the jet is ignited, a flame starts propagating downward and its vertical position (height) is stabilized at a location where the flame speed becomes equal to the jet velocity with the opposite sign. Thus, a laminar lifted aerosol flame is produced. Note that in this configuration, as well as any configuration involving moving aerosol, the speed of particles entering the flame could slightly differ from the speed of the gas flow because of the slip. Moreover, even if a flame is ignited in a stagnant aerosol (dust cloud), thermal expansion, thermophoresis, and other processes could induce motion of the aerosol ahead of the flame so that the speed of particles and gas would differ. Thus, the flame speed for an aerosol could be based on either particle or gas velocity in the cold aerosol jet entering the flame. As discussed later, the measurements in this paper are relying on the particle velocity, whereas the possible slip effects are described and quantified.

Flame Shape

Produced flames had characteristic, cylindrically symmetric shape similar to a candle flame, which is a very unusual geometry for the flame speed measurements. As already noted, the aerosol jet was issued from a 0.8-mm nozzle. As the jet decelerated, it slightly expanded to 1–1.5 mm. Apparently because of the thermal expansion, the observed flame diameter (horizontal dimension) varied in a range of 2–3 mm. The flame vertical dimension was 2–5 mm, and the flames were lifted 2–50 mm above the nozzle. Figure 2 shows characteristic shapes of an aluminum aerosol flame using images taken with long exposure times to outline the flame clearly. (The interiors of the flame in these images are overexposed.) Figure 2 shows that, although the flame is very narrow, most of the particles ignite on a flat, horizontal surface, which can be called the leading edge of the flame. For the small, lifted flames, the leading edge of the flame was clearly visible (Fig. 2) unlike for the Bunsen cone, where it is blocked from the direct view.[6–9] Streaks of particles in the unburned jet are illuminated by the flame and also visible in Fig. 2. One can see that particles near the jet center enter the flame with velocities directed normal to its leading edge. Because the flame was stabilized at a particular location, detailed observations of the flame structure could be readily made optically, unlike for a flame traveling through a stagnant aerosol in a tube, for example, in microgravity experiments.[11]

Aerosol Mass Concentration Measurement

To measure the aerosol mass concentration, glass-fiber filters mounted in a filter holder connected to a vacuum line were placed above the burning aerosol jet for 15-s time periods. The weight of the combustion products collected during this time was determined by weighing each filter before and after the sampling. A second filter was mounted above the first one in several experiments aimed to determine how effectively the first filter collects the combustion products. No mass change of the second filter could be detected, indicating that the first filter captured essentially all of the condensed combustion products. The experiments were repeated for different settings of the high-voltage power supply affecting the aerosol number density. Flame speed measurements were performed, as described later, simultaneously with the product collection to obtain a correlation between the aerosol mass concentration and flame speed. The experimental mass concentrations were determined for Al aerosol assuming that the combustion products consisted of pure Al_2O_3. The assumption of the complete conversion of Al into the oxide was verified by x-ray phase analysis of the collected products in which only minute amounts of unburned aluminum were detected. It was found that the mass concentrations of aerosols for which laminar flames could be produced and sustained were in the range of about 0.4–1.4 kg/m^3.

Advantages and Disadvantages of LLFAB

One of the most significant advantages of the LLFAB technique for production of laminar aerosol jets is its ability to operate with a wide range of materials and powders of different sizes. (As with any other technique, very fine and ultrafine powders are increasingly difficult to aerosolize because of the strong interparticle adhesion forces.) The ability to handle different materials is especially important for characterization of many practically interesting novel metallic fuels, for example, mechanical alloys and coated powders. The only limitation on the material is that it should be at least mildly conductive to ensure electric charge exchange between particles and capacitor plates. Aerosol flames have been produced in our preliminary experiments with Al, Mg, Zr, and Ti, and aerosol jets were formed with silicon and glass beads, although for glass beads, maximum achievable concentrations were lower than for other materials, apparently, because of their very low conductivity. The aerosol flames were stabilized with powders having volume mean diameters in the range of 5–50 μm.

Unlike for techniques producing aerosol in a fluidized bed, particle agglomeration is insignificant in LLFAB because each particle is independently lifted by its interaction with charged plates and because any agglomerates are being destroyed by multiple particle–plate collisions.

The produced flames were very narrow, causing both advantages and disadvantages at the same time. The main advantage is that a narrow flame is optically transparent, enabling a variety of optical diagnostics, for example, pyrometry, imaging, light absorption, spatially resolved spectroscopy, etc., to be readily applicable. In

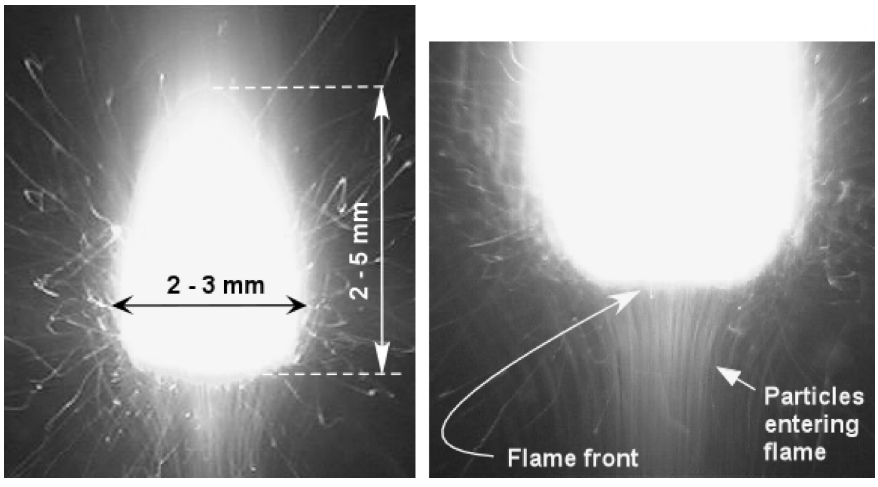

Fig. 2 Characteristic shape of aluminum aerosol flame produced using LLFAB, nozzle size 0.8 mm; streaks of particles entering flame illuminated by the flame's own radiation: a) overall flame shape and typical dimensions and b) closeup where the flame leading edge is clearly visible.

addition, the radiative heat transfer between the optically thin flame and aerosol jet is expected to be insignificant.

Another advantage of a small-scale flame is that only 0.5–1 g of powder is sufficient to establish a laminar flame and carry out necessary measurements. This advantage is crucial when dealing with new materials available in small quantities. The disadvantages are that the diffusion of ambient gas in the flame as well as heat transfer from the sides of the flame are significant. Therefore, the stoichiometry of the mixture is well defined only in the cold aerosol, and the flame temperature might be affected by additional heat losses. However, the importance of these effects on the flame propagation rate is unclear. The stoichiometry of any aerosol flame (in terms of an oxidizing environment surrounding burning particles) is always poorly defined within its extended flame zone: Smaller particles ignite and burn rapidly, leaving larger particles burning in a leaner environment. Additional oxidizer diffusion in a narrow, elongated flame could accelerate the burn rate of such larger particles. However, the accelerated burn rate for larger particles would not produce a significant increase in the metal aerosol flame temperature, which is usually lower than the adiabatic flame temperature and is limited by radiation heat losses sharply increasing with temperature. Thus, no strong changes are expected in the temperature profile in the preheat zone directly affecting the flame speed. Radiative heat losses are very strong in any aerosol flames, and it has been observed that most of the radiated energy is lost and does not preheat aerosol even for larger Bunsen-type flames.[7] Therefore, additional heat losses from the flame sides are unlikely to alter significantly the aerosol temperature and flame speed that is primarily defined by the particle ignition processes. Indeed, analyses of the experimental results discussed subsequently indicate that the flame speeds measured using LLFAB for metal aerosols are comparable to the burning velocities for similar aerosols measured using other techniques.

Flame Speed Measurement Technique

Characterization of Aerosol Jet Velocity Profiles Using Laser Light Scattering

If the vertical velocity profile for the produced aerosol jet is known, the position of the lifted flame can be used to determine the flame speed. To determine the jet velocity profiles for different experimental conditions, a vertical laser sheet was projected on the cold aerosol jet to illuminate the particle trajectories. Images of the illuminated trajectories were taken using a digital video camera with a specified exposure time, so that the length of each streak divided by the exposure time gave the local aerosol velocity. An example of a jet image taken using the laser sheet illumination is shown in Fig. 3. The values of Reynolds number Re estimated for the jet at different experimental flowrates varied from 30 to 90. The particle streaks were nearly parallel, as shown in both Figs. 2 and Fig. 3; no recirculations and eddies were observed in aluminum and magnesium aerosol flame images (Fig. 2) as discussed and shown later. Therefore, the laminar nature of the gas flow and the flame were clearly established.

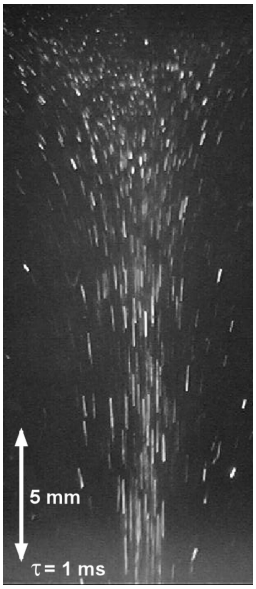

Fig. 3 Aluminum aerosol jet produced using electrostatic fluidization technique, illuminated by a He–Ne laser sheet, exposure time $t = 1$ ms: particle steak lengths used to detemine aerosol jet velocity as a function of vertical coordinate.

Characterization of Aerosol Jet Velocity Profiles Using Laser Doppler Velocimetry

The information about the vertical velocity profiles in the aerosol jet was further supported using laser Doppler velocimetry (LDV) measurements. In addition, the information regarding the uniformity of particle velocities at different heights was obtained, which is especially important for experiments with polydisperse aerosols.

A Dantec® Flowlite one-dimensional (He–Ne laser based, wavelength 632.8 nm) apparatus was used. The LDV measurements were made for two flow rates, selected to be at the minimum and maximum values of the flow rate range used for the flame speed measurements in this work. An example of the measured particle velocity distributions for an Al aerosol at three different vertical positions is shown in Fig. 4. Immediately above the nozzle, the particle velocity distribution is quite broad, indicative of a wide range of the initial velocities for particles exiting the plate capacitor. However, the velocity distribution of the particles in the aerosol jet narrows down rapidly, and the velocities are nearly uniform at the heights of 10 mm and above. This was the range of the vertical positions used for the flame speed measurements in this work.

The absolute values of the cold-jet velocities measured at different heights using LDV agreed well with the previously described measurements using the laser light scattering.

A possible effect of the flame on the aerosol jet velocity profile was investigated by comparing the particle velocity distributions at different jet heights obtained from the LDV measurements with and without flame. It was observed that the aerosol jet is not affected by the flame at the distances of ~2 mm and below from the flame's leading edge. This distance coincides with the estimated width of the flame preheat zone within which the temperature increases rapidly affecting the jet structure. To eliminate the effect of the jet preheating on the flame speed measurement, one would need to identify the flame position at the beginning of the preheat zone. However, this was impractical because this location could only be obtained from the detailed, spatially resolved temperature measurements. Instead, the location of the flame's leading edge readily obtained from the processing of the flame video images was considered to indicate the flame position. Therefore, a small systematic error associated with the flame's preheat zone thickness was present in all of the measurements reported in this paper.

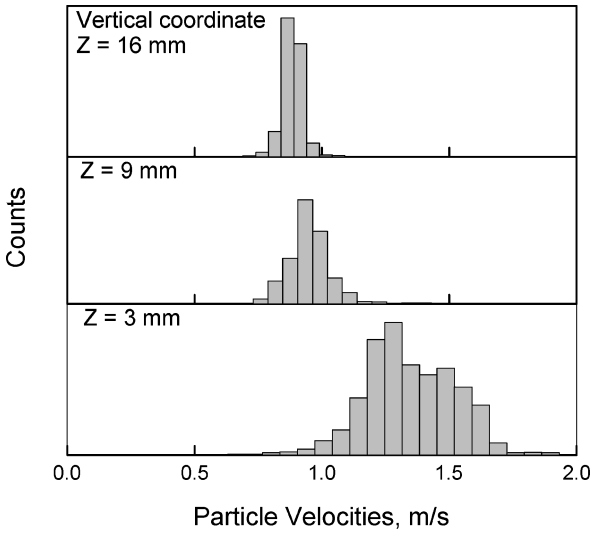

Fig. 4 Distributions of particle velocities at different jet heights measured using LDV: Al 10–14 μm by Alfa Aesar, initial jet velocity at the nozzle, $v_0 = 2.06$ m/s.

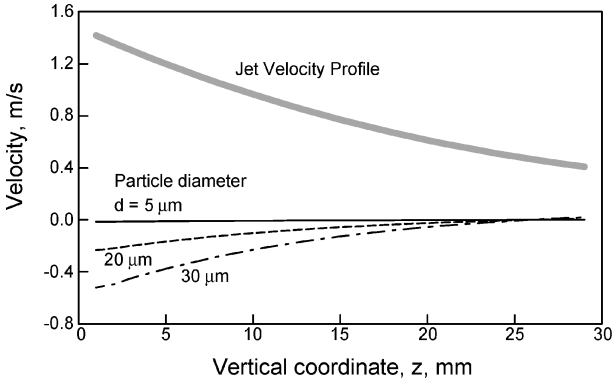

Fig. 5 Experimental velocity profile for cold-aerosol jet ($v_0 = 2.06$ m/s) and estimated slip velocities for different size aluminum particles as function of jet height.

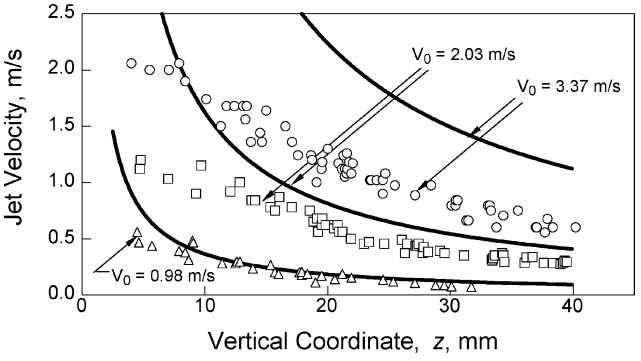

Fig. 6 Experimental vertical jet velocity profiles for three different jet velocities at the nozzle, v_0 (or, respectively, different gas flow rates), and respective gas jet velocity profiles predicted theoretically using Eq. (2) for centerline jet velocity decay.[24]

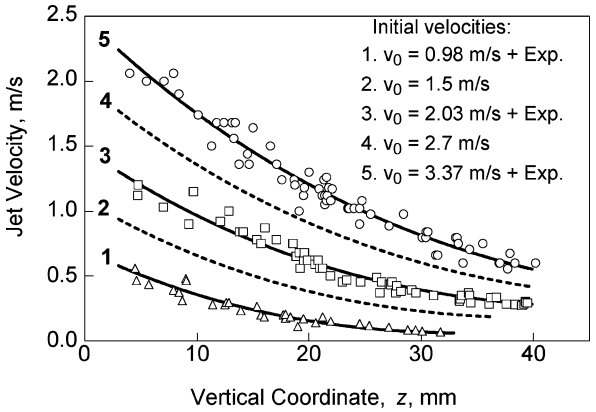

Fig. 7 Experimental vertical jet velocity profiles for three different jet velocities at nozzle, v_0, as shown in Fig. 6 and respective curves $v = f(z, v_0)$ computed using an empirical formula (3), for the same three values of jet velocities at the nozzle. Also curves predicted using Eq. (3) for two intermediate values of v_0 are shown.

Effect of Particle Slip

An effect of the particle slip was evaluated considering the acceleration a implied from the measured vertical velocity profiles of the aerosol jet. Because both experimental techniques described earlier tracked velocity of the aerosol particles, the acceleration a directly reflected the particle motion. Therefore, assuming that the drag force is described by the Stokes formula, the particle slip velocity v_{slip} can be readily estimated using the equation of particle motion:

$$ma = mg - 3\pi\eta d v_{\text{slip}} \tag{1}$$

where m and d are the particle mass and diameter, respectively, g is the gravitational constant, and η is the air viscosity. Examples of the estimated slip velocities for the particles of different sizes as a function of the vertical coordinate are shown in Fig. 5 along with a typical experimental jet velocity profile used for this estimate. This estimate shows that the slip effects are negligible for the flame speeds under 0.5 m/s for all particle sizes. It also shows that the slip effects could be large for coarse particles and for the high flame speeds. For such cases, the slip correction needs to be used if the flame speed measurements reported here and based on the particle velocities are compared to the measurements relying on the aerosol gas velocity. Note also that the correction could be smaller for nonspherical particles for which the drag force is stronger. In addition, for a polydisperse aerosol, the slip correction could be different for different particle sizes.

Calibrations of Jet Velocity Profiles and Flame Speed Measurements

For routine calibration of the jet velocity profiles, a laser light scattering technique was used. The jet images were obtained at different gas flow rates and, thus, different initial jet velocities at the nozzle. For each flow rate, a series of jet images, similar to that shown in Fig. 3, were taken and processed. The aerosol jet velocity profiles were determined for the range of heights of 2–50 mm above the nozzle, that is, locations overlapping with the range of heights of 10–50 mm, where the aerosol flames were stabilized in further experiments. In a series of tests, the jet velocity profiles were measured for different powders used to produce aerosol flames in this work. These measurements showed that the jet velocity profiles for different powders coincided with one another within the experimental scatter.

Initially, the measured aerosol jet velocity profiles were compared with the gas jet velocity profiles predicted theoretically. An expression for dimensionless centerline velocity decay for a laminar gas jet[24] was used:

$$v = \left(0.375 \cdot \rho \cdot v_0^2 \cdot r^2\right) \Big/ \mu \cdot 1/z \tag{2}$$

where v is the gas velocity at the center of the jet at the height z above the nozzle, ρ is the density of air, v_0 is the gas velocity at the nozzle ($z = 0$), r is the nozzle radius, and μ is the air viscosity.

Examples of the experimental and theoretically computed velocity profiles are shown in Fig. 6. The discrepancy between the experimental and theoretical curves for all but the smallest nozzle velocity, $v_0 = 0.98$ m/s, could be attributed to the momentum exchange between the aerosol particles and gas. Also note that Eq. (2) is not expected to describe well the jet velocity profile in the proximity of the nozzle. Because the analysis of momentum transfer in a cold jet was outside the scope of this project, the experimental jet velocity profiles shown in Fig. 6 were used directly as calibration data for the flame speed measurements. An empirical formula was derived that described the jet velocity v as a function of the vertical coordinate z, with the initial jet velocity v_0 as a parameter:

$$v = \frac{-0.02008v_0^2 + 8.497v_0 + 0.8818}{0.2319z + 7.751} - 0.2516v_0 - 0.3187 \tag{3}$$

In this formula, velocities are in meters per second, and coordinate is in millimeters. It was developed using a curve-fitting function of a commercial data processing application (PsiPlot, version 6a for Windows by Poly Software International, Inc.). The solid lines in Fig. 7 show the computed trends predicted using the empirical formula (3) for the three experimental values of v_0. Respective local measured jet velocities are also shown in Fig. 7. A good match between the experimental and the computed trends is observed. The ability of Eq. (3) to predict reasonably the jet velocity profiles for the initial velocities, for example, gas flow rates, used to produce flames but for which no cold-jet velocity profile measurements were conducted, was additionally assessed. Trends of $v = f(z, v_0)$ estimated using Eq. (3) for the intermediate values of v_0 are shown in Fig. 7 by dashed lines and are located, just as expected, between the respective best-fit curves for the adjacent measured values of v_0. Thus, it

was observed that the found empirical formula was well behaved in the entire range of values of v_0 covered in the experiments.

Preliminary experiments with the aerosol flames showed that a single measurement of flame position could be misleading in identifying the flame speed due to a number of potential errors. For example, the difference in the heat exchange between the flame and the parts of the burner at different flame heights, nonuniformity in the horizontal jet velocity profile, and an error in defining the position of the flame's leading edge for a small, two-dimensional flame could contribute to significant misrepresentation of the flame speed.

To minimize these errors, a single-point flame location measurement was replaced with an experimentally determined trend describing the vertical flame positions as a function of the gas flow rate. Although gas flow rate was varied directly in experiments, because the theoretical treatment of the jet, for example, in Ref. 24 the nozzle velocity v_0 is used, the following discussion is also using nozzle velocity determined for each experimental flow rate from the gas mass conservation,

$$v_0 = W/\pi r^2 \tag{4}$$

where W is the gas flow rate through the nozzle of radius r.

The approach for flame speed measurements is based on an assumption that the (downward) flame speed v_f remains constant when the nozzle velocity v_0 changes. Thus, when the location z_f where the aerosol moves with the velocity of $-v_f$ (directed upward in the decelerating aerosol jet) shifts, the flame position should adjust accordingly. An experimental trend of $z_f(v_0)$ was obtained systematically varying the nozzle velocity v_0 and, at the same time, measuring the vertical flame position z_f,. For the reproducible jet geometry, and flame speed independent of the flow rate, this trend should be completely defined by the values of the flame speed v_f and jet velocity profile as a function of v_0, that is, Eq. (3).

This approach is illustrated by tracking the flame positions for two fractions of the size-classified Mg powders. The powder samples were prepared by sieving commercial Alfa Aesar Mg −325 mesh powder. Measured flame positions at different nozzle velocities are shown in Fig. 8. The horizontal error bars show the accuracy of the rotameter used to measure the flow rate and an estimated error of its calibration. The vertical error bars are due to the short time fluctuations in the measured vertical flame position. The final step in the procedure is to determine whether a single value of v_f, defined by empirical Eq. (3), matches the experimental trend $z_f(v_0)$ for each powder, and if yes, what this v_f value is. To find the flame speed from the experimental data directly, the empirical formula (3) was reversed to express $z = z_f$ as a function of v_0, with, v_f used as an adjustable parameter:

$$z_f = \frac{-0.02008v_0^2 + 6.546v_0 - 7.751v_f - 1.588}{0.05836v_0 + 0.2319v_f + 0.07391} \tag{5}$$

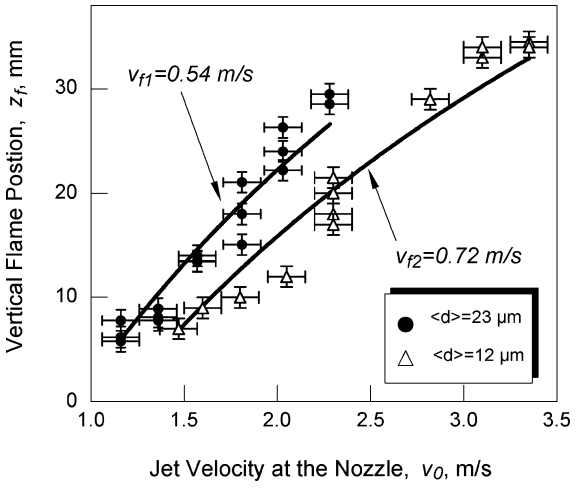

Fig. 8 Experimental flame positions as a function of initial jet velocity for two magnesium powder samples with different size distributions. Solid curves show best fits produced using Eq. (5).

Expression (5) served as an input for the curve-fitting routine and was used to find the flame speed v_f for which the experimental curves $z_f(v_0)$, could be matched.

The curve fits found for each of the two observed experimental trends for two fractions of Mg powder are shown in Fig. 8. A reasonably good agreement between the measured flame positions and the empirical curves shown in Fig. 8 indicates that flame speeds can indeed be determined from the experimental $z_f(v_0,)$ curves. Note that the found flame speeds do not noticeably depend on the nozzle velocity, or flow rate, unlike the measurements using Bunsen burner.[9] Matching the entire curve, rather than a single experimental point, significantly minimizes the effect of some scatter in the experimental results and the effect of other potential errors. Therefore, a higher quality measurement is produced.

The specific result presented in Fig. 8 confirms and quantifies a generally expected trend that the flame propagates faster through an Mg aerosol when the particle size becomes finer.

Results and Discussion

Flame Speed Measurements for Al Aerosols

Most of the relevant results presented in the current literature deal with aluminum aerosol combustion; therefore, experiments in this work were also conducted with aluminum aerosol. Two types of spherical aluminum powders were used in these experiments, their characteristics are given in Table 1. The powders will be referred to using their respective manufacturer's identification. Particle sizes were determined using a Coulter LS 230 enhanced laser diffraction particle size analyzer. In addition, specific surface areas of the powders were determined by nitrogen absorption employing the Brunauer–Emmett–Teller (BET) isotherm using a high-speed gas sorption analyzer, NOVA 3000.

The effect of the aerosol mass concentration on the measured flame speed was investigated for the aluminum powder X-65. Aerosol flames were produced in air. The results of the flame speed measurements for different aerosol mass concentrations are shown in Fig. 9. Respective equivalence ratios are also shown in Fig. 9. The horizontal error bars are due to some scatter in the experimental weights of the powder samples collected in the filter, as well due to an error in the flow rate measurement. The vertical error bars are due to the scatter in the observed experimental flame positions and respective flame speeds. Only fuel-rich flames could be produced in these experiments, in agreement with our earlier reports.[21,23] For the first time, laminar flames were established with the very high aerosol mass concentrations, shown in Fig. 9. A slow decrease in the measured flame speed at increased mass concentrations can be qualitatively explained by an increased heat capacity of a more concentrated aerosol jet. At the same time, in a narrower range of mass

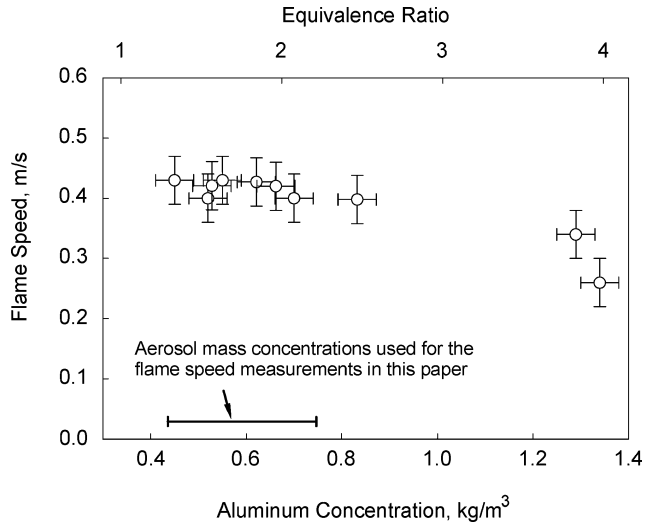

Fig. 9 Effect of aluminum aerosol mass concentration in air on flame speed measured using LLFAB.

concentrations of about 0.45–0.75 kg/m^3, which was used in all of the experiments described later, the effect of the mass concentration on the flame speed is negligible. This last observation is consistent with the conclusion of very weak dependence of the flame speed on aerosol concentration made earlier based on the Bunsen burner measurements for fuel-rich aerosols[6–8] conducted with relatively narrow mass concentration ranges.

To investigate the effect of the particle size and burner geometry on the measured flame speed, experiments were conducted with two nozzles, 0.8 and 1.6 mm diam, and with both types of spherical aluminum powders (Table 1) aerosolized in air. The results of these experiments are presented in Table 2. The results of flame speed measurements were reasonably well reproducible for each nozzle size and each powder type. As expected, and similar to the results mentioned earlier for Mg powder (Fig. 8), the measured flame speed for the finer X-65 powder was higher than for the coarser 10–14-μm powder. An effect of the nozzle size on the measured flame speed was detected for the 10–14-μm powder, whereas the flame speed appeared not to change as a function of the nozzle size for the X-65 powder. At the same time, it was noticed that, for larger size flames produced with the 1.6-mm nozzle with the X-65 powder, the flame shape was no longer cylindrically symmetric. Examples of the flame images produced with the X-65 and 10–14-μm powders with the 1.6-mm nozzle are shown in Fig. 10. Note that the flame's leading edge for the X-65 powder is no longer normal to the vertical aerosol jet as it is for 10–14-μm powder and for smaller flames (Fig. 2). Thus, for such larger flames, a correction could be needed to interpret the flame speed measurements based on the vertical flame position. Although this effect may need to be investigated further, all other measurements reported in this paper have been made with a smaller 0.8-mm nozzle and, respectively, smaller, cylindrically symmetric flames.

To compare the produced flame speed measurements with the reported previously burning velocities, a dependency of aluminum aerosol flame speed on the oxygen concentration was measured, similar to the measurements by Goroshin et al.[8] and Ballal.[11] Nitrogen/oxygen mixtures with different oxygen concentrations were prepared, and experiments with both types of aluminum powders were conducted (with a 0.8-mm nozzle). The results of these experiments are presented in Fig. 11 along with the earlier burning velocity measurements.[8,11] The horizontal error bars show inaccuracy in the prepared mixtures due to the pressure gauge errors. The vertical error bars, as before, indicate a scatter in the measured vertical flame positions. Because the higher flame propagation rates are expected for finer particles, results of our measurements produce a reasonable trend considered together with the microgravity flame tube measurements[11] using coarser aluminum powder. In both cases, an increase in the flame speed is observed at higher oxygen concentrations, and the flame speed is increasing for finer particles for the same gas composition. The measurements produced using the Bunsen burner also show an increase in the flame speed at increased oxygen concentrations; however, the reported burning velocities are lower than would be expected from our measurements when the very fine particle sizes used in Ref. 8 are considered. It is unclear just

Table 2 Effect of nozzle diameter on the aerosol flame measurement using LLFAB

Run	Nozzle diameter, mm	Manufacturer powder	Flame speed, m/s
1	0.8	X-65	0.35
2	0.8	X-65	0.41
3	0.8	10–14 μm	0.25
4	0.8	10–14 μm	0.27
5	0.8	10–14 μm	0.28
6	1.6	X-65	0.40
7	1.6	10–14 μm	0.15
8	1.6	10–14 μm	0.21

Table 1 Aluminum powders used in aerosol flame experiments and their parameters determined using LALLS and the BET methods

Manufacturer	Powder	Mean diameter, based on volume distribution, by LALLS, μm	Mean diameter, based on area distribution, by LALLS, μm	Sauter mean diameter, μm	Specific surface area by BET, m^2/g	Equivalent BET diameter, μm
Toyal America	X-65	10.87	7.40	23.45	0.46	4.92
Alfa Aesar	10–14 μm	20.33	16.28	31.70	0.41	5.41

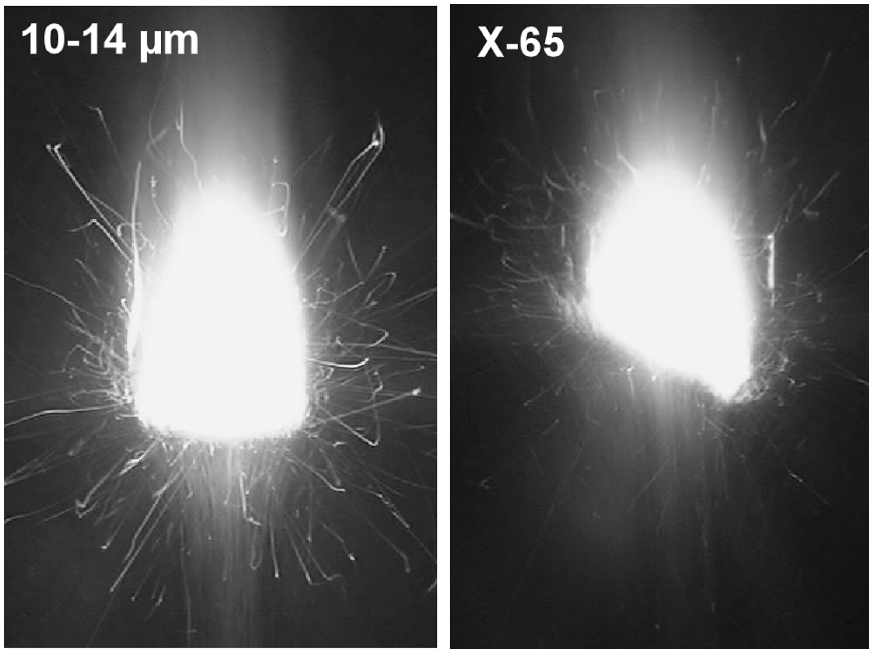

Fig. 10 Flames with aerosols of X-65 and 10–14-μm aluminum powders produced with the 1.6-mm nozzle: flame of X-65 powder does not appear cylindrically symmetric; flame leading edge is not normal to the aerosol jet.

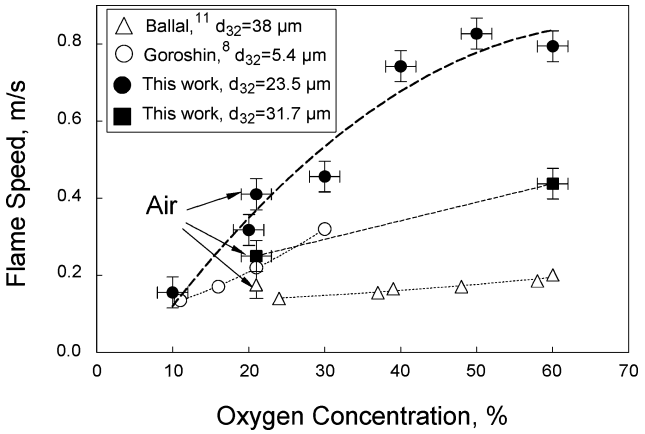

Fig. 11 Effect of oxygen concentration in oxygen/nitrogen gas mixtures on aluminum aerosol flame speed. Filled symbols show measurements produced in this work using LLFAB. Open symbols show results currently reported in the literature[8,11] and produced using different experimental techniques. Reference particle sizes are described using Sauter mean diameter d_{32}.

how significant this discrepancy is because of the reported changes in the Bunsen burner burning velocity measurements as a function of both the burner diameter[6,8] and gas flow rate.[8]

In summary, the flame speed measurements for Al powder aerosols using LLFAB have been well reproducible and have shown qualitatively expected trends for the flame speed as a function of aerosol mass concentration, oxygen concentration, and particle sizes. Therefore, it is possible to use LLFAB both as a tool for evaluation of combustion of metallic powders and as an experimental setup for studying physical and chemical processes of aerosol flames.

Flame Speed Measurements for Al-Based Mechanical Alloys

LLFAB was used to evaluate novel metallic fuels prepared using mechanical alloying. The preparation and properties of the mechanical alloy powders tested in this work are described elsewhere[23,25] and are only briefly summarized here. Mechanical alloying was used to synthesize sets of samples in the systems Al–Mg, Al–Zr, Al–Ti, Al–Li, Al–C, and Al–Mg–H. X-ray diffraction, electron microscopy, and low-angle laser diffraction were used to characterize sample structures, phase compositions, morphologies, and particle size distributions, respectively. The produced materials were nanocrystalline metastable phases with particle sizes in the range of 1–100 μm. For most systems, the crystallite sizes vary from 4 to 50 nm; the elemental compositions were uniform throughout the sample and corresponded to the bulk composition of the initial powder mixture. The formation of thermodynamically stable intermetallic phases during mechanical alloying was suppressed by selecting appropriate process parameters.

Two sets of mechanically alloyed powders were evaluated. The first set included a series of Al–Mg alloys with Mg concentration varied from 10 to 50 at.%. Measured flame speeds for these alloys were compared vs reference Al and Mg powders with particle size distributions similar to those of the alloys. The second set of alloys comprised compositions with 90 at.% of Al and 10% of an alloying element, that is, Ti, Zr, Li, C, or MgH_2. A flame speed measured for an Al aerosol served as a reference point for these materials.

The particle size distributions for each of the tested samples, including reference Al (10–14 μm by Alfa Aesar) and Mg (–325 mesh by Alfa Aesar) powders are shown in Figs. 12 and 13. Representative examples of the scanning electron microscope images of the powders are shown in Fig. 14. The particle sizes of all powders are generally comparable to one another, and the powder surface morphologies of all mechanical alloys are qualitatively similar.

Laminar lifted flames were produced with all of the described powders aerosolized in air, and representative images of the flames

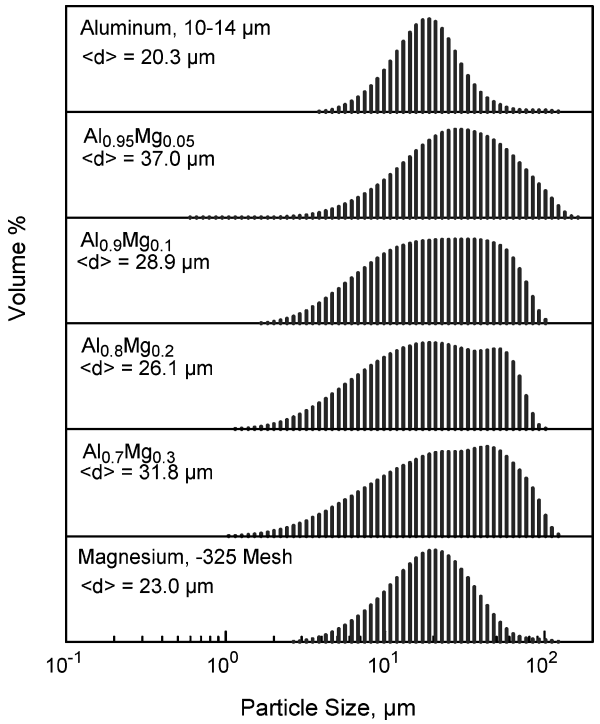

Fig. 12 LALLS particle size distributions for Al–Mg mechanical alloys and respective reference aluminum and magnesium powders; values of mean diameters based on volume distributions.

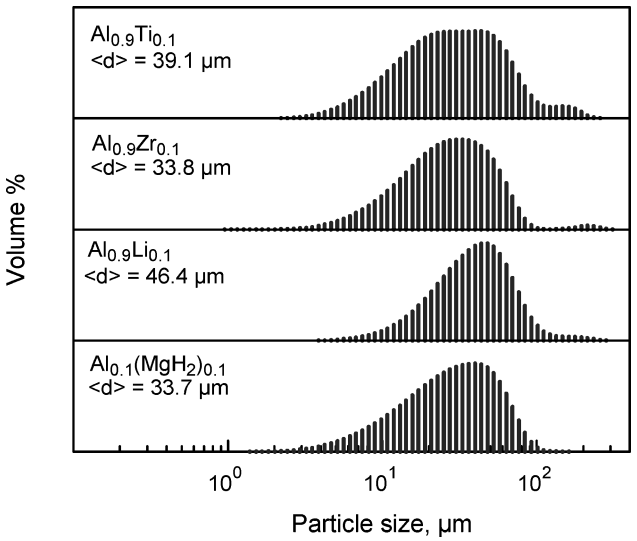

Fig. 13 Low-angle laser light scattering particle size distributions for aluminum-based mechanical alloys with 10 at.% of alloying element.

with different aerosols are shown in Fig. 15. All of the images in Fig. 15 were taken with the exposure time of 10 ms and aperture size reduced to visualize the structure and streaks of the particles within the flame, unlike the images in Figs. 2 and 10 showing only the outlying flame shapes. The flame structure and particle streaks are remarkably different for different alloys and for pure metals. Most of the particle streaks are directed vertically and appear diffused in the pure aluminum flame, indicating a laminar flame structure and a strong vapor-phase reaction shielding individual particles. The flame images for all of the mechanical alloys indicate pronounced heterogeneous reactions with bright particle streaks and asymmetric burning producing dashed and curved streaks. The asymmetry is especially significant for the flames of Al–Ti and Al–Zr alloys, where the directions of the particle streaks change randomly during the lifetime of each burning particle.

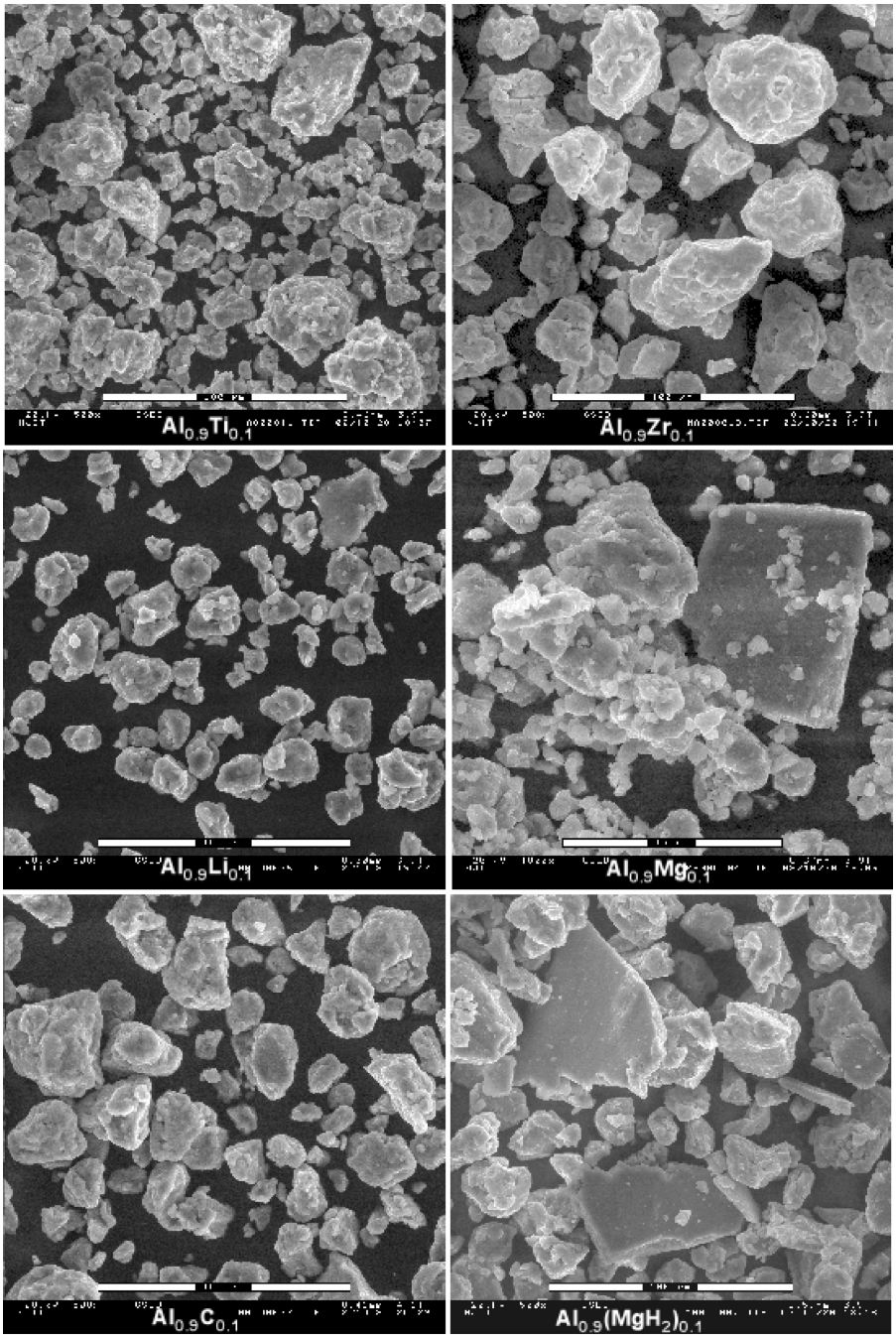

Fig. 14 Different alloy powders, scanning electron microscope images. Scale bar is 100 μm for all images except for $Al_{0.9}Mg_{0.1}$ alloy, where scale bar is 40 μm.

Before the flame propagation rates are compared for different materials, note that for all of the alloys the mass concentrations used in these experiments were in a range of 0.6–0.8 kg/m^3. As was observed for aluminum aerosols (Fig. 9), in this range of mass concentrations, the flame speeds were found to be essentially independent on the aerosol number density. This observation, consistent with the experimental data by other researchers,[6–8] allowed us to assume that a fair comparison of the measured flame speeds for different materials could be produced while the aerosol mass concentrations remained in the above range.

The results of our flame speed comparisons for aerosols of pure aluminum, pure magnesium, and a range of metastable Al–Mg mechanical alloys are shown in Fig. 16. As earlier, the vertical error bars are due to some scatter in the measured vertical flame positions. It is interesting that some of the Al-Mg alloys exhibited flame speed exceeding that of pure magnesium, in spite of somewhat coarser average particle size, making these alloys very attractive for applications requiring a high metal fuel burn rate combined with a high volumetric reaction enthalpy.

The results of the flame speed measurements for the second set of aluminum alloys (with 10% of different alloying element each) are shown in Fig. 17. The flame speeds measured for different alloy aerosols are relatively close to one another, but all are higher than the speed of the pure aluminum aerosol flame. Once again, note that the particle sizes of the alloys were relatively coarse, and thus, even a small increase in the flame speed is significant. Note that it was impossible to establish a laminar lifted flame for an aluminum–10% carbon alloy that was also prepared and tested, even though single particles were observed to ignite and burn. The experimentation with the $Al_{0.9}C_{0.1}$ alloy generally indicated that the flame speed for this material is lower than that of the pure aluminum and slower than the range with which the LLFAB was designed to work.

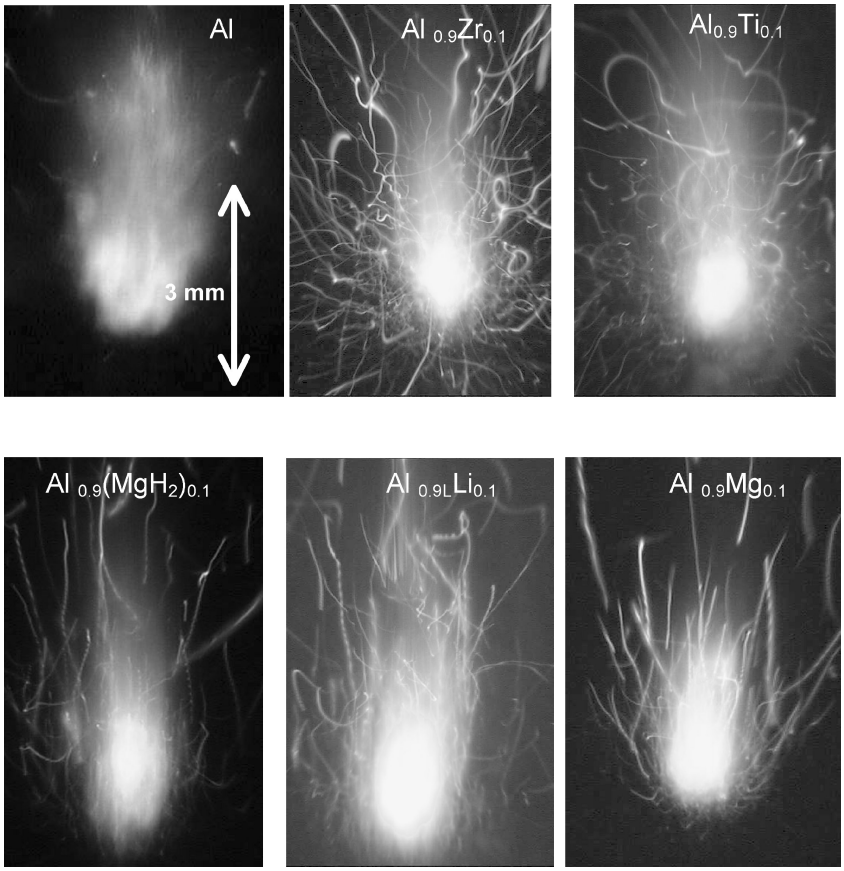

Fig. 15 Lifted laminar aerosol flames of aluminum and different aluminum-based mechanical alloys; 10-ms exposure time.

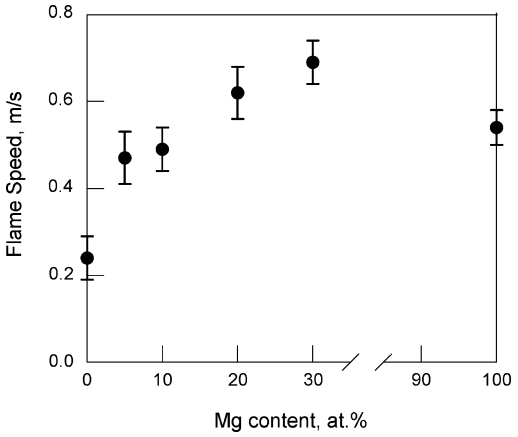

Fig. 16 Experimental flame speeds for aerosols of pure aluminum, average particle size $\langle d_{Al} \rangle = 20.3$ μm, pure magnesium $\langle d_{Mg} \rangle = 23.0$ μm, and a range of metastable Al–Mg mechanical alloys with average particle sizes in the range of $\langle d_{alloys} \rangle = 30.1 \pm 4$ μm.

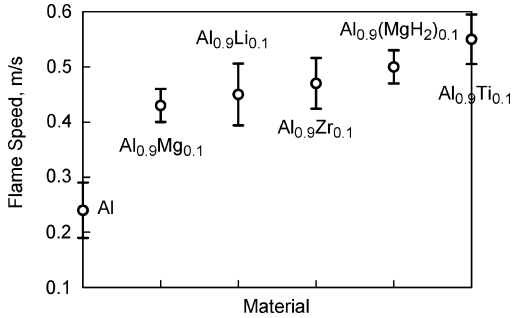

Fig. 17 Experimentally detemined flame speeds for aerosols of pure aluminum powder and aluminum-based alloys with 10 at.% of alloying element.

Conclusions

This research established an experimental methodology of measuring the flame propagation speed in metal particle aerosols. The methodology is based on a novel burner, LLFAB, using electrostatic fluidization and enables one to measure flame propagation speeds accurately for a wide range of metals and metal-based materials. Main advantages of the new experimental methodology are its abilities to handle powders with different size distributions, create and maintain laminar aerosol flames in a wide range of mass concentrations, and use only very small amounts of powders for the flame measurements. Experiments showed that, in spite of unusual flame geometry in LLFAB, qualitatively similar trends for aerosol speed as a function of oxygen concentration, particle size, and mass concentration could be obtaned with LLFAB as were reported earlier using Bunsen burner and aerosol flame propagating in a tube in microgravity. The effects of aluminum and magnesium particle size distributions on the flame speed in respective metal–air aerosols were quantified. The effect of the aluminum aerosol mass concentration on the flame speed was investigated in the range of mass concentrations of 0.4–1.4 kg/m^3. A decrease in the flame speed at higher mass concentrations was observed, even though this effect was negligible in the range of 0.45–0.8 kg/m^3 used for the rest of the reported experiments. The developed technique was used to compare the flame speeds for pure aluminum and magnesium powders vs flame speeds for a set of aluminum-based mechanical alloys with Mg, Ti, Zr, Li, MgH_2, and C as alloying elements. It was observed that the flame speeds for all of the tested alloys, except the one with carbon, are higher than the flame speed in the pure aluminum aerosol. It was also observed that for some of the Al–Mg mechanical alloys, the flame speeds exceeded that of pure magnesium even though the particle sizes of the alloy powders were coarser than those of magnesium.

Acknowledgments

This work was supported in part by the Office of Naval Research, Grant N00014-00-1-0446, Judah Goldwasser; Department of Navy,

Crane Division, Award N00164-02-C-4702, Robert Shortridge; and Defense Threat Reduction Agency, Award DTRA01-02-C-0064, John Kolts. Additional support was provided by the New Jersey Commission on Science and Technology, Award 01-2042-007-24.

References

[1]Choudhury, P. R., and Gerstein, M., "Feasibility of Programmed Ignition of Metal Compounds in a Scramjet," *Acta Astronautica*, Vol. 36, No. 7, 1995, pp. 379–386.

[2]Chan, M. L., Reed, R., and Ciaramitaro, D. A., "Advances in Solid Propellant Formulations," *Solid Propellant Chemistry, Combustion and Motor Interior Ballistics*, edited by V. Yang, T. B. Brill, and W. Z. Ren, Vol. 185, Progress in Astronautics and Astronautics, AIAA, Reston, VA, 2000, pp. 185–206.

[3]Glassman, I., *Combustion*, 3rd ed., Academic Press, San Diego, CA, 1996, pp. 125–162.

[4]Kuo, K. K., *Principles of Combustion*, Wiley, New York, 1986, pp. 315–322.

[5]Cassel, H. M., Das Gupta, A. K., and Guruswamy, S., "Factors Affecting Flame Propagation Through Dust Clouds," U.S. Bureau of Mines, Vol.-Date 7, Pittsburgh, PA, Sept. 1948, pp. 185–190.

[6]Cassel, H. M., "Some Fundamental Aspects of Dust Flames," U.S. Bureau of Mines, Rept. of Investigation 6551, Pittsburgh, PA, Nov. 1964.

[7]Goroshin, S. V., Shoshin, Y. L., Ageyev, N. D., and Poletayev, N. I., "The Premixed Aluminium Dust Flame Structure," *Flame Structure*, Vol. 1, Nauka, Novosibirsk, Russia, 1991, pp. 213–218.

[8]Goroshin, S., Fomenko, I., and Lee, J. H. S., "Burning Velocity in Fuel-Rich Aluminum Dust Clouds," *Twenty-Sixth Symposium (International) on Combustion*, Combustion Inst., Pittsburgh, PA, 1996, pp. 1961–1967.

[9]Goroshin, S., Kolbe, M., and Lee, J., "Burning Velocity Measurements in Aluminum-Air Suspensions Using Stabilized Dust Flames," *Sixth International Microgravity Combustion Workshop*, NASA CO-2001-210826, 2001, pp. 221–224.

[10]Goroshin, S., Bidabadi, M., and Lee, J. H. S., "Quenching Distance of Laminar Flame in Aluminum Dust Clouds," *Combustion and Flame*, Vol. 105, 1996, pp. 147–160.

[11]Ballal, D. R., "Flame Propagation Through Dust Clouds of Carbon, Coal, Aluminum and Magnesium in an Environment of Zero Gravity," *Proceedings of the Royal Society of London, Series A: Mathematical, Physical and Engineering Sciences*, Vol. 385, No. 1788, 1983, pp. 21–51.

[12]Alekseev, A. G., Barlas, R. A., Tsidelko, T. I., and Shapoval, A. F., "Effect of Particle Size on the Combustibility and Explosion Parameters of Dispersed Aluminum and Magnesium Powders," *Preduprezhdenie Vnezapnykh Vzryvov Gazodispersnykh Sist*, edited by V. V. Nedin, 1971, pp. 66–73 (in Russian).

[13]Belyaev, A. F., Frolov, Y. V., and Korotkov, A. I., "Combustion and Ignition of Particles of Finely Dispersed Aluminum," *Fizika Goreniia i Vzryva*, Vol. 4, 1968, pp. 323–329 (in Russian).

[14]Brossard, C., Ulas, A., Yen, C. L., and Kuo, K. K., "Ignition and Combustion of Isolated Aluminum Particles in the Post-Flame Region of a Flat-Flame Burner," *16th International Colloquium on the Dynamic of Explosions and Reactive Systems*, Kraków, Poland, 1997, p. 22.

[15]Assovskiy, I. G., Zhigalina, O. M., and Kolesnikov-Svinarev, V. I., "Gravity Effect in Aluminum Droplet Ignition and Combustion," *Fifth International Microgravvity Combustion Workshop*, NASA Conf. Publ., 1999, URL: http://www.ncmr.org/events/combustion1999/proceedings.html.

[16]Johnson, C., Parr, T., Hanson-Parr, D., Hollins, R., Fallis, S., and Higa, K., "Combustion and Oxidation of Metal Nanoparticles and Composite Particles," *Proceedings of 37th JANNAF Combustion Subcommittee Meeting*, Chemical Propulsion Information Agency, Columbia, MD, 2000, pp. 539–551.

[17]Bucher, P., Yetter, R. A., Dryer, F. L., Vicenzi, E. P., Parr, T. P., and Hanson-Parr, D. M., "Condensed-Phase Species Distributions About Al Particles Reacting in Various Oxidizers," *Combustion and Flame*, Vol. 117, No. 1-2, 1999, pp. 351–361.

[18]Dreizin, E. L., "Experimental Study of Stages in Aluminum Particle Combustion in Air," *Combustion and Flame*, Vol. 105, 1996, pp. 541–556.

[19]Li, S. C., and Williams, F. A., "Ignition and Combustion of Boron in Wet and Dry Atmospheres," *Twenty-Third (International) Symposium on Combustion*, Combustion Inst., Pittsburgh, PA, 1990, pp. 1147–1154.

[20]George, P., and DesJardin, P. E., "Towards a Mechanistic Model for Aluminum Particle Combustion," American Society of Mechanical Engineers, ASME Heat Transfer Paper HT2003-47499, July 2003.

[21]Shoshin, Y., and Dreizin, E., "Production of Well-Controlled Laminar Aerosol Jets and Their Application For Studying Aerosol Combustion Processes" *Aerosol Science and Technology*, Vol. 36, 2002, pp. 953–962.

[22]Colver, J. M., "Dynamics of an Electric (Particulate) Suspension," *Advances in the Mechanics and the Flow of Granular Materials*, edited by M. S. Shahinpoor, Vol. 1, Gulf, Houston, TX, 1983, pp. 355–373.

[23]Shoshin, Y. L., Mudryy, R. S., and Dreizin, E. L., "Preparation and Characterization of Energetic Al-Mg Mechanical Alloy Powders," *Combustion and Flame*, Vol. 128, 2002, pp. 259–269.

[24]Turns, S. R., *An Introduction to Combustion*, 2nd ed., McGraw–Hill, Boston, 2000, pp. 306–311.

[25]Schoenitz, M., Dreizin, E. L., and Shtessel, E., "Constant Volume Explosions of Aerosols of Metallic Mechanical Alloys and Powder Blends," *Journal of Propulsion and Power*, Vol. 19, No. 3, 2003, pp. 405–412.

A. Karagozian
Associate Editor